Hybrid silencers with micro-perforated panels and internal partitions

Xiang Yu, Li Cheng,[a] and Xiangyu You
Department of Mechanical Engineering, The Hong Kong Polytechnic University, Hung Hom, Kowloon, Hong Kong, China

(Received 11 September 2014; revised 1 December 2014; accepted 8 December 2014)

A sub-structuring approach, along with a unit cell treatment, is proposed to model expansion chamber silencers with internal partitions and micro-perforated panels (MPPs) in the absence of internal flow. The side-branch of the silencer is treated as a combination of unit cells connected in series. It is shown that, by connecting multiple unit cells with varying parameters, the noise attenuation bandwidth can be enlarged. With MPPs, the hybrid noise attenuation mechanism of the silencer is revealed. Depending on the size of the perforation hole, noise attenuation can be dominated by dissipative, reactive, or combined effects together. For a broadband sound absorption, the hole size, together with the perforation ratio and other parameters, can be optimized to strike a balance between the dissipative and reactive effect, for ultimately achieving the desired noise attenuation performance within a prescribed frequency region. The modular nature of the proposed formulation allows doing this in a flexible, accurate, and cost effective manner. The accuracy of the proposed approach is validated through comparisons with finite element method and experiments.
 [http://dx.doi.org/10.1121/1.4906148]

[NX] Pages: 951–962

I. INTRODUCTION

Acoustic silencers as noise control devices are widely used. Passive acoustic silencers are roughly classified into reactive, dissipative, and hybrid type through their combined effects. In the presence of internal cross-sectional discontinuities, reactive silencers attenuate sound by reflecting its energy back to the upper-stream, mainly in the low-to-mid frequency range. Typically, a simple expansion chamber provides periodic dome-like Transmission Loss (TL) pattern below the cutoff frequency, but the existence of TL dips due to chamber axial length may deteriorate the overall performance. In order to alleviate these deficiencies, internal partitions can be used inside the chamber, as reported in the literature.[1–5] For example, Selamet and Ji[1] investigated circular expansion chambers with extended inlet and outlet using an analytical approach, which was later extended to dual-chamber[2] and multi-chamber[3] silencers. Lee and Kim[4] attempted to improve the sound attenuation performance of reactive silencers with internal partitions through topology optimization, by considering the reduction of flow loss simultaneously.[5] Another type of reactive silencer is based on acoustic resonators.[6–8] Howard *et al.*[6] proposed an exhaust stack silencer with slot-type rhomboid shaped resonators. Wang and Mak[7] studied the sound wave propagation in a duct lined with periodic resonators array. Seo and Kim[8] optimized the arrangement of resonator arrays for broader low-frequency band noise reduction. Meanwhile, a so-called plate silencer with side-branch cavity covered by flexible plates has been developed,[9] which works effectively in the low-to-mid frequency range with properly tuned plate parameters and boundary conditions.

On the other hand, dissipative silencers achieve sound attenuation by means of energy dissipation, mainly targeting the mid-to-high frequency range. This type of silencer typically consists of an expansion volume filled with fibrous materials, whose acoustic behavior can be characterized by a complex sound speed and density using a bulk-reacting model.[10] In practice, fibrous linings are usually protected by a perforated duct, which also helps reduce the flow loss. The acoustic impedance of the added perforated lining in contact with fibrous material and its influence on the silencing performance has also been investigated.[11,12] Since pure dissipative silencers cannot provide adequate sound attenuation in the low frequency range due to the limitation of material property, various hybrid silencers have been proposed to compensate for the low frequency deficiency.[13–16] For example, Ji[13] analyzed a straight through hybrid silencer consisting of a concentric folded resonator with a dissipative chamber using the boundary element method (BEM). Wu *et al.*[14–16] studied various packed silencer configurations using BEM analysis, with different internal surfaces being characterized as regular, perforated, bulk-reacting interfaces. Generally speaking, hybrid silencers can provide a broader TL than reactive or dissipative silencers alone.

In recent years, micro-perforated panel (MPP) absorbers have attracted much attention as promising alternatives to traditional sound absorbing materials. A MPP typically consists of a thin sheet with distributed perforation holes in sub-millimeter size. Its acoustic impedance can be reasonably well predicted using a model developed by Maa,[17] which regards the small perforation hole as a lattice of short narrow tubes, with an end correction term being added to account for the attached air mass on both ends. Conventional MPP

[a]Author to whom correspondence should be addressed. Electronic mail: li.cheng@polyu.edu.hk

absorbers usually require a backing cavity to create a Helmholtz resonance effect. The dependence of the absorption performance of MPPs on various parameters has been discussed.[17] Apart from the normal incidence, studies on MPP absorbers under more complex working conditions, such as irregular-shaped backing cavity,[18] oblique incidence,[19] or in coupled vibroacoustic environment,[20] etc., have also been reported in the literature. Owing to the nonfibrous, incombustible, and cleanable feature, MPP absorbers have found their uses in a wide range of engineering applications.[21–28] For example, Asdrubali and Pispola[21] proposed noise barriers using transparent polycarbonate MPPs, which exhibit appealing acoustical and optical performances. Park[22] investigated the acoustic behavior of MPP absorbers backed by a Helmholtz resonator for low-frequency performance improvement, and examined its applicability in reducing the noise level inside a launcher fairing. Herrin *et al.*[23,24] attempted to enhance the MPP absorption in a rectangular enclosure by partitioning the backing cavity with a honeycomb structure, aiming at applications in construction equipment, building, and acoustic silencers.

The initial attempt of using MPPs for noise control inside a duct was made by Wu,[25] where the MPP surface is considered as a locally reacting boundary. As such, a MPP together with the backing cavity is treated as an equivalent absorptive surface, whose impedance can be calculated using the formula given in Ref. 17. However, due to the limitation of this assumption, the predicted results were not accurate enough compared with experiments. More recently, Allam and Abom[27,28] proposed a new type of dissipative silencer based on MPPs, which delivers comparable silencing performance to a dissipative silencer filled with porous materials. In the aforementioned studies, although differences exist among different designs, MPPs are used mainly as dissipative elements. One could wonder that, depending on the hole size of the MPPs and properly arranged backing chambers, whether MPPs might also bring about the reactive effect of the silencers to achieve a well-balanced hybrid effect. In a more general sense, a thorough understanding of the role that MPPs might play in more complex acoustic systems such as silencers is still lacking in the literature.

Figure 1 shows a typical silencer with an expansion volume covered by MPPs, and with solid partitions inside the backing cavity. For such systems, conventional modeling techniques based on one-dimensional theory[25,27] are limited by the higher-order mode propagation, while analytical modeling based on a modal approach and an interface matching technique[1,2] can become very tedious in coping with system complexity. It is noted that due to these limitations, the sound attenuation mechanism of MPP silencers has not been fully apprehended in the literature. In order to tackle the problem, this paper proposes a three-dimensional (3D) substructuring approach based on the Patch Transfer Function (PTF) method[29–32] to deal with MPP silencers with internal partitions. In the proposed approach, the side-branch is modeled as a combination of multiple unit cells, each comprising a MPP facing and an acoustic backing cavity. The major objectives of the present study are to capture the hybrid noise attenuation mechanism, to analyze the possible influences of system parameters, and to provide guidelines for the design of such silencers.

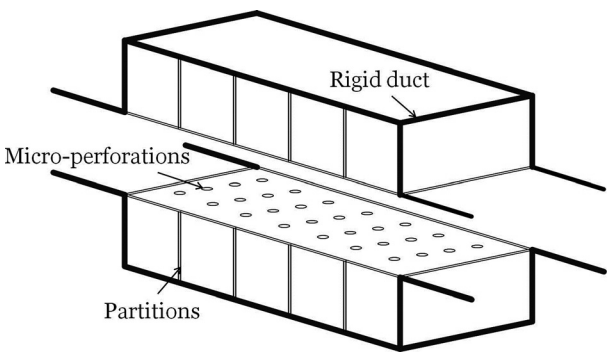

FIG. 1. Expansion chamber silencer with micro-perforated panels and internal partitions.

Following this introduction, the proposed PTF formulation together with the unit cell treatment is presented. Reactive silencers with only internal partitions are first discussed to serve as benchmarks, which are shown to exhibit narrow band TL characteristics. By combining multiple unit cells with varying parameters together as a resonator array, the TL performance and the bandwidth can be generally improved in the selected frequency range. The acoustic behavior after adding a MPP to the reactive chamber is then investigated, and the hybrid effect combining both sound reflection and absorption is analyzed. The study shows that there exists considerable room for possible performance optimization by properly balancing the hybrid effects of the proposed MPP silencers. Using the proposed approach, this can be done by tuning various parameters of the MPPs at a very low computational cost. The accuracy and convergence of the calculations are validated through comparisons with the finite element method (FEM) and experiments.

II. FORMULATION

Consider the straight-through MPP silencer as shown in Fig. 1. The solid partitions behind a MPP sub-divide the side-branch cavity into multiple chamber units. The substructuring treatment of the global system is illustrated in Fig. 2, where the silencer domain is decoupled into inlet/outlet ducts, main chamber, and two side-branches. The main chamber is connected with the adjacent acoustic domains through four coupling interfaces numbered from 1 to 4. Based on the concept of the PTF approach,[29–32] each coupling interface between adjacent acoustic domains is meshed into N elementary areas called patches, whose optimal meshing size to ensure the calculation convergence has been discussed in Ref. 29. Thus, the total numbers of patches being divided at the four interfaces are N_1, N_2, N_3, and N_4, respectively.

At each coupling interface, the patch transfer functions (PTFs) are used as subsystem couplers, which are defined as the average response at a receiving patch due to an excitation at another patch. In describing the coupling interface of an acoustic domain, patch impedance Z_{ij}^{a} is generally used,

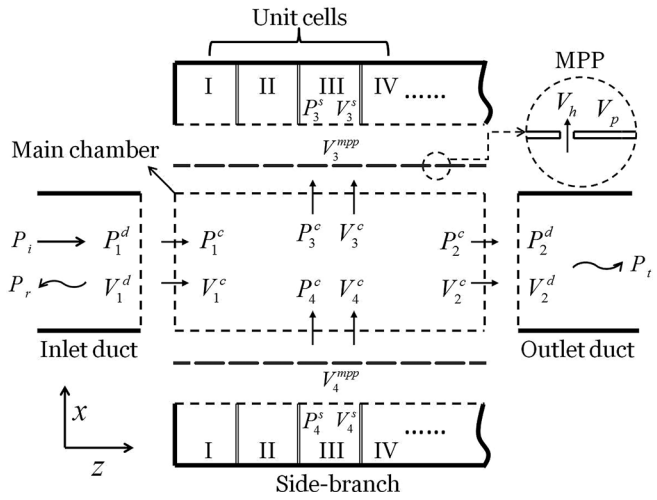

FIG. 2. Sub-structuring treatment of the system using the PTF approach.

while for a vibrating structural interface, using patch mobility Y^s_{ij} is more convenient,

$$Z^a_{ij} = \frac{\bar{F}^a_i}{\bar{V}^a_j}, \quad \text{where } \overline{V^a_j} = \frac{1}{S_j}\int_{s_j} V^a dS_j \text{ and } \overline{F^a_i} = \int_{S_i} P^a dS_i,$$
$$Y^s_{ij} = \frac{\bar{V}^s_i}{\bar{F}^s_j}, \quad \text{where } \overline{V^s_i} = \frac{1}{S_i}\int_{s_i} V^s dS_i \text{ and } \overline{F^s_j} = \frac{1}{S_j}\int_{S_j} F^s dS_j, \tag{1}$$

where i and j represent the receiving and exciting patch, S_i and S_j are the corresponding surface areas, and superscripts s and a denote the structural and acoustic quantities, respectively. Note that the subsystem PTF at an interface with N patches is a $N \times N$ square matrix, $\bar{V}$ and $\bar{F}$ are both $N \times 1$ vectors.

The PTF coupling framework for the present MPP silencer is similar to that of a reactive silencer as presented in Ref. 32. The subsystem PTFs to be determined are summarized as follows: Duct radiation impedances Z^d at interfaces 1 and 2; 16 surface-to-surface impedances Z^c for the main chamber; side-branch cavity impedances Z^{sc} and MPP surface mobilities Y^{sc} at interfaces 3 and 4, respectively. Note that all these quantities are, *a priori*, calculated before the assembly to form a set of databases. Then, according to the normal direction notations in Fig. 2, the equations to describe the fully coupled system in the linear regime are established as[32]

$$\begin{aligned}
&\tilde{F} + Z^d_1 V^d_1 = Z^c_{11} V^c_1 + Z^c_{12} V^c_2 + Z^c_{13} V^c_3 + Z^c_{14} V^c_4,\\
&Z^c_{21} V^c_1 + Z^c_{22} V^c_2 + Z^c_{23} V^c_3 + Z^c_{24} V^c_4 = Z^d_2 V^d_2,\\
&Y^{sc}_3 (Z^c_{31} V^c_1 + Z^c_{32} V^c_2 + Z^c_{33} V^c_3 + Z^{sc}_3 V^{sc}_3 + Z^c_{34} V^c_4) = V^{sc}_3,\\
&Y^{sc}_4 (Z^c_{31} V^c_1 + Z^c_{32} V^c_2 + Z^c_{43} V^c_3 + Z^c_{44} V^c_4 + Z^{sc}_4 V^{sc}_4) = V^{sc}_4,
\end{aligned} \tag{2}$$

where patch forces at interfaces 1 and 2 between the main chamber and inlet/outlet ducts are required to be continuous; the coupling between the main chamber and side-branch cavities is formulated by treating MPP as a structural interface.

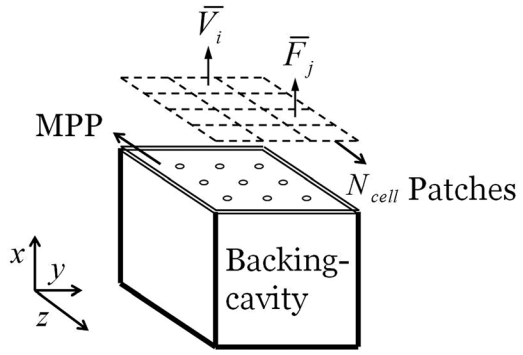

FIG. 3. A unit cell with a MPP facing and a backing acoustic cavity.

The PTF calculations of conventional subsystems, including duct and main chamber impedance, have been detailed in Ref. 32. Here, the remaining challenge comes from the modeling of the side-branch cavity. In Fig. 2, the side-branch cavity can be viewed as a series of unit cells, each comprising a MPP facing and a backing rectangular cavity. Note that the dimensions and MPP parameters of each unit cell can be different. As shown in Fig. 3, the interface separating the main chamber and the cell cavity is also segmented into N_{cell} patches, where the cavity impedance and MPP mobility are determined. As such, the total number of patches at interfaces 3 and 4 is a sum of patches contributed from all the cells:

$$\begin{aligned}
N_3 &= N^{\text{I}}_3 + N^{\text{II}}_3 + N^{\text{III}}_3 + N^{\text{IV}}_3 + \cdots,\\
N_4 &= N^{\text{I}}_4 + N^{\text{II}}_4 + N^{\text{III}}_4 + N^{\text{IV}}_4 + \cdots,
\end{aligned} \tag{3}$$

where roman numeral superscripts are used to identify the unit cells in Fig. 2.

The side-branch impedance Z^{sc} and mobility Y^{sc} are obtained by combining all the unit cells to form an element array. For the modeling of the MPP in a unit cell, the hole impedance formula by considering the perforated holes as a lattice of short narrow tubes gives[20]

$$\begin{aligned}
Z_h = \frac{32\eta t}{d^2}&\left[\left(1+\frac{k^2}{32}\right)^{1/2} + \frac{\sqrt{2}}{32}k\frac{d}{t}\right]\\
&+ j\rho_0\omega t\left[1+\left(1+\frac{k^2}{32}\right)^{-1/2} + 0.85\frac{d}{t}\right],
\end{aligned} \tag{4}$$

where ρ_0 is the air density, η is the air viscosity, t and d are the thickness and hole diameter of MPP, $k = d\sqrt{\rho_0\omega/4\eta}$. The term $0.85d/t$ is used to characterize the end correction effect.

If the panel frame of MPP is rigid, the averaged air velocity in the vicinity of MPP surface V_{MPP} can be obtained by averaging the vibrational velocity inside the perforated holes with the rigid panel frame as

$$V_{\text{MPP}} = \sigma V_h, \tag{5}$$

where V_h is the air velocity inside the holes, and σ is the perforation ratio.

When a pressure difference is subjected to both sides of the MPP surface, the hole mass velocity is expressed as

$$\Delta p = Z_h V_h. \tag{6}$$

Since the distance between perforated holes is much larger than their diameters and the panel frame is not vibrating, the cross-coupling between patches among a MPP surface is generally weak. Thus, the MPP mobility of a unit cell is a diagonal matrix ($N_{\text{cell}} \times N_{\text{cell}}$), with corresponding diagonal terms equal to

$$Y_{\text{MPP}} = \frac{V_{\text{MPP}}}{\Delta p \times S} = \frac{\sigma}{Z_h S}, \tag{7}$$

where S is the surface area of the segmented patch.

In practice, a MPP is usually made of a thin metal sheet. If the panel is flexible, its flexural vibration has to be taken into account. According to Eq. (1), the flexural panel vibration being subjected to a pressure difference can be expressed as $V_p = Y_p(\Delta p \times S)$, where Y_p is the panel structural mobility.[33] The averaged MPP velocity in Eq. (5) is then an average of the air mass velocity inside holes V_h, and the vibrating velocity of panel frame V_p,

$$V_{\text{MPP}} = (1-\sigma)V_p + \sigma V_h. \tag{8}$$

The pressure difference across the MPP is contributed by the viscous force and inertial force together. The former depends on the relative motion between the air mass and panel frame, while the latter depends on the air mass velocity only,[20]

$$\Delta p = \text{Re}\{Z_h\}(V_h - V_p) + j\text{Im}\{Z_h\}V_h, \tag{9}$$

where Re{} and Im{} represent the real and imaginary parts of the complex hole impedance.

Since the perforation ratio of MPP is typically very low, by neglecting the influence of a small perforated area on the panel vibration, the equivalent MPP mobility can be calculated as

$$Y_{\text{MPP}} = \left[(1-\sigma) + \frac{\sigma \text{Re}(Z_h)}{Z_h}\right] Y_p + \frac{\sigma}{Z_h S}. \tag{10}$$

The above equation describes not only the effect of micro-perforation, which is a diagonal matrix related to hole impedance and porosity, but also the cross-coupling between patches through the panel flexural vibration. Note that Eqs. (7) and (10) are identical when the panel frame is rigid, i.e., Y_p is a null matrix.

As to the modeling of the backing-cavity behind MPP, the present formulation considers it as a 3D rectangular cavity. Based on the modal expansion theory, the sound pressure field inside the cavity can be analytically decomposed into modal coordinates:

$$p_c(x,y,z) = \sum_r a_c^r \varphi_c^r, \tag{11}$$

where a_c^r is the rth modal amplitude of the cavity, φ_c^r is the corresponding eigenfunction, and the x axis depicts the cavity depth direction, as shown in Fig. 3.

The rigid-walled acoustic modes as eigenfunctions are adopted here, whose calculation accuracy has been thoroughly validated in the literature,[30,33]

$$\varphi_c^r = \cos\left(\frac{r_x \pi}{L_x^c} x\right)\cos\left(\frac{r_y \pi}{L_y^c} y\right)\cos\left(\frac{r_z \pi}{L_z^c} z\right), \quad r_x, r_y, r_z = 0, 1, 2, ..., \tag{12}$$

where r_x, r_y, r_z are the modal indices in the x, y, z directions, and L_x^c, L_y^c, L_z^c are the corresponding cavity dimension.

The Green's formula together with Helmholtz equation is used to relate the cavity variables and boundary conditions in an integral expression. The normal directions are defined as pointing outward in Fig. 3,

$$\int_{V_c} (p_c \nabla^2 \varphi_c^r - \varphi_c^r \nabla^2 p_c) dV_c = \int_{S_c} \left(p_c \frac{\partial \varphi_c^r}{\partial n} - \varphi_c^r \frac{\partial p_c}{\partial n}\right) dS_c, \quad \nabla^2 p_c + k^2 p_c = 0. \tag{13}$$

Substituting the pressure gradient of a vibrating boundary $(\partial p_c/\partial n) = -j\rho_0 \omega \bar{V}_n$ into the above equation, the cavity modal amplitude can be calculated as

$$a_c^r N_c^r (k^2 - k_r^2) = \int_{S_c} (j\rho_0 \omega \bar{V}_n) \varphi_c^r dS_c, \tag{14}$$

where the cavity resonances $k_r^2 = k_x^2 + k_y^2 + k_z^2$, $N_c^r = \int_{V_c} \varphi_c^r \varphi_c^{r'} dV_c$. $\bar{V}_n$ is the averaged normal velocity at an excitation patch.

Then, according to Eq. (1), the backing-cavity impedance of a unit cell, which is a $N_{\text{cell}} \times N_{\text{cell}}$ matrix, can be obtained as

$$Z^c = \frac{\bar{F}_i^c}{\bar{V}_j^c} = \sum_r \frac{j\rho_0 \omega}{N_c^r (k^2 - k_r^2)} \int_{S_i} \varphi_c^r dS_i \int_{S_j} \varphi_c^r dS_j. \tag{15}$$

So far, the cavity impedance and MPP mobility of an elementary unit cell at the coupling interface has been formulated using Eqs. (10) and (15). Since the unit cells are well separated from each other by the rigid partitions, the side-branch mobility Y^{sc} and impedance Z^{sc} at interfaces 3 and 4 can be constructed by combining all the unit cells as a common subsystem:

$$Y^{sc} = \begin{bmatrix} Y_{\text{mpp}}^{\text{I}} & & & \\ & Y_{\text{mpp}}^{\text{II}} & & \\ & & Y_{\text{mpp}}^{\text{III}} & \\ & & & \ddots \end{bmatrix}; \quad Z^{sc} = \begin{bmatrix} Z_c^{\text{I}} & & & \\ & Z_c^{\text{II}} & & \\ & & Z_c^{\text{III}} & \\ & & & \ddots \end{bmatrix}. \tag{16}$$

In addition to Eq. (2), the system response at each coupling interface is obtained by applying the velocity continuity condition at the connecting patches:

$$V_1^d = V_1^c, V_2^c = V_2^d; \text{ at interfaces } 1, 2,$$
$$V_3^c = V_3^{sc}, V_4^c = V_4^{sc}; \text{ at interfaces } 3, 4\,. \tag{17}$$

Then, the systematic equations in Eq. (2) can be rearranged into

$$[\boldsymbol{M}]\{\boldsymbol{V}\} = \{\boldsymbol{F}\}, \tag{18}$$

where

$$M = \begin{bmatrix} (Z_{11}^c - Z_1^d) & Z_{12}^c & Z_{13}^c & Z_{14}^c \\ Z_{21}^c & (Z_{22}^c - Z_2^d) & Z_{23}^c & Z_{24}^c \\ Y_3^s Z_{31}^c & Y_3^s Z_{32}^c & Y_3^s (Z_{33}^c + Z_3^{sc}) - I & Y_3^s Z_{34}^c \\ Y_4^s Z_{31}^c & Y_4^s Z_{32}^c & Y_4^s Z_{43}^c & Y_4^s (Z_{44}^c + Z_4^{sc}) - I \end{bmatrix};$$
$$V = \{ V_1^c \quad V_2^c \quad V_3^c \quad V_4^c \}; \; F = \{ \tilde{F} \quad 0 \quad 0 \quad 0 \}.$$

As shown in Fig. 2, the sound pressure field inside the inlet duct is a combination of incident and reflected sound waves, and that inside the outlet duct is the transmitted sound waves. Once the patch velocity response has been solved, the silencing performance can be evaluated by calculating the sound TL,

$$\mathrm{TL} = 10 \log_{10}\left(\frac{1}{\tau}\right), \tag{19}$$

where τ is the ratio between the transmitted and incident sound power $\tau = \Pi_2^t / \Pi_1^i$.

The incident sound power Π_i^1 at interface 1 corresponding to a normal plane wave incidence with pressure amplitude equal to p_0 is

$$\Pi_i^1 = \frac{|p_0|^2}{2\rho_0 c_0} S_1, \tag{20}$$

where S_1 is the total surface area of the incident surface. As to the transmitted sound power due to patch vibration at interface 2,

$$\Pi_2^t = \frac{1}{2}\int_{S_2} \mathrm{Re}\{P_2 \times V_2^*\} dS_2, \tag{21}$$

where P_2 is the radiated sound pressure into the outlet duct, calculated via duct radiation impedance Z^d as $P_2 = Z^d V_2$; S_2 is the area of the radiation surface; the asterisk for the patch velocity denotes its complex conjugate.[32]

In order to reveal the hybrid mechanism of a MPP silencer, the reactive effect and dissipative effect need to be separated. The reflection and absorption coefficients are used to quantify these effects. The reflection coefficient R is defined as the reflected sound power over the incident power at interface 1,

$$R = \frac{\Pi_1^r}{\Pi_1^i} = \frac{(\Pi_1^i - \Pi_1^t)}{\Pi_1^i}, \tag{22}$$

where the reflected sound power Π_1^r is calculated by subtracting the incident power Π_1^i [Eq. (20)] and transmitted power Π_1^t to the downstream, at interface 1:

$$\Pi_1^t = \frac{1}{2}\int_{S_1} \mathrm{Re}\{P_1 \times V_1^*\} dS_1. \tag{23}$$

Similarly, the absorption coefficient α is defined as the percentage of sound power being absorbed by the silencer, which writes

$$\alpha = \frac{(\Pi_1^t - \Pi_2^t)}{\Pi_1^i}. \tag{24}$$

It is clear that the present 3D modeling does not suffer from the plane wave assumption, which is an inherent limitation in the previous analyses on MPP silencers.[25,27] Meanwhile, the proposed concept of unit cell provides a flexible tool to handle complex side-branch configurations, which could eventually allow a free-tuning of silencing performance in the design stage.

III. NUMERICAL ANALYSES

The proposed sub-structuring formulation is employed to investigate the acoustic behavior of several typical silencer configurations based on Fig. 1. The main objective is to capture the hybrid noise attenuation mechanism, and to provide some practical design guidelines. The basic silencer configuration is a rigid expansion chamber with a dimension of $0.3\,\mathrm{m}(x) \times 0.1\,\mathrm{m}(y) \times 0.5\,\mathrm{m}(z)$, and the cross-section of the inlet/outlet duct is $0.1\,\mathrm{m}(x) \times 0.1\,\mathrm{m}(y)$.

A. Reactive silencers with internal partitions

Before considering the effects of MPPs, reactive silencers with only internal partitions are first studied to serve as benchmarks. In Fig. 4, the chamber length, being kept as 0.5 m, is evenly divided into several sub-chambers by certain pairs of solid partitions, while the central airway

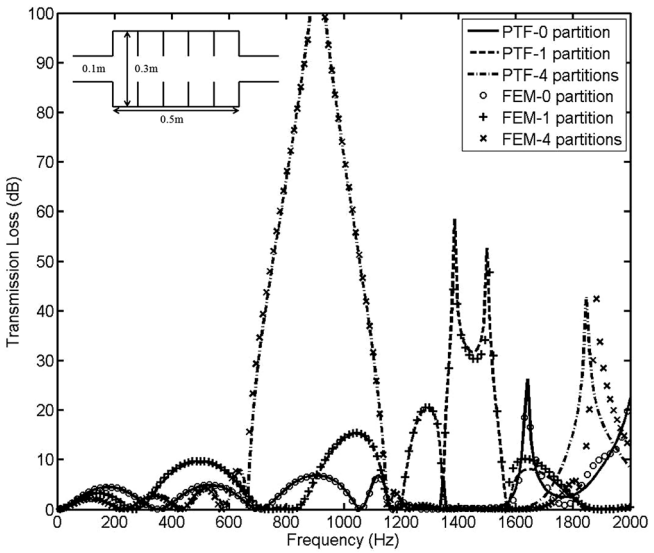

FIG. 4. TL of reactive silencers with internal partitions: Comparison with FEM analyses.

is left open for the purpose of air passage. Figure 4 compares the predicted TLs using the present PTF approach with those obtained from FEM analyses using commercial software COMSOL. In all three silencer cases with single, dual, and five chambers, respectively, excellent agreements are observed between PTF curves and FEM results, which validate the proposed formulation. Phenomenon-wise, the attenuation performance of the simplest empty chamber is rather weak in the entire frequency range. For the five-chamber silencer, the predicted TL shows a pronounced sharp peak near 930 Hz, at the expense of compromising the TL performances at other frequencies. This sharp TL peak is actually due to the accumulative effect of connecting multiple identical unit cells in series, forming a kind of resonator array. The resonant frequency of each resonator cell is located at 930 Hz.

As shown in Fig. 5, the reflection and absorption coefficients, defined in Eqs. (22) and (24), are used to quantify the reactive effect and dissipative effect. For the two cases, the overall trend of the reflection coefficient coincides with the corresponding TL curve, while the absorption coefficients are constantly zero. This means that the attenuation mechanism of such silencers is purely reflective.

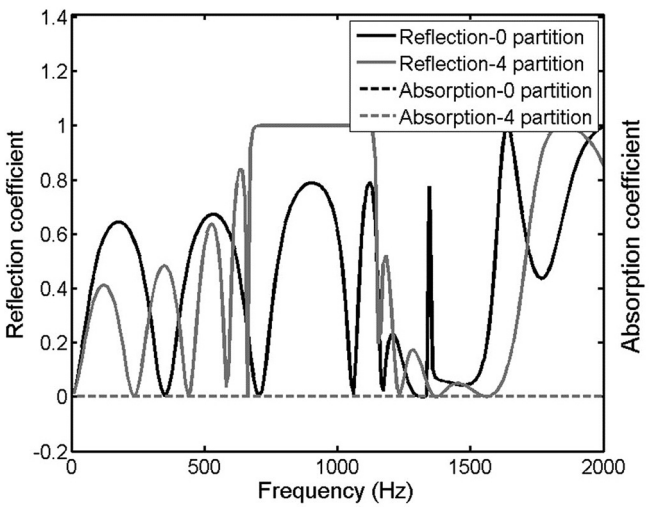

FIG. 5. Reflection and absorption coefficient of the reactive silencers calculated using the PTF approach.

The accumulative effect of resonator cells indicates the possibility of improving TL performance by connecting multiple unit cells with varying dimensions. The principle is verified using the silencer configuration shown in Fig. 6. Along the duct side-wall, five unit cells with varying depths ranging from 0.1 to 0.3 m are attached, in a random sequence. The PTFs of each cell is pre-calculated and stored in a database, allowing a flexible modeling of the system. The predicted TL curves corresponding to three different cell sequences are presented in Fig. 6. It can be seen that, irrespective of the sequence, the resonant peaks attributed to each unit cell can be clearly identified. By combining different unit cells, the attenuation bandwidth is significantly widened, which is desirable for broadband noise control applications. This comparison also shows that different cell sequences also impact the TL, which can be further optimized using the proposed approach at a very low computational cost.

Through the present example, the advantage of bringing the concept of unit cell into silencer design is demonstrated. In the design stage, the performance of such silencer can be quickly estimated by studying the acoustic stop bands provided by each unit cell. By combining different unit cells with optimized TLs to cover distinct frequency bands, the overall attenuation performance can be greatly enhanced within a prescribed frequency region.

B. Hybrid silencers with partitions and MPPs

By adding MPPs, the combined effect of internal partitions with MPPs is first studied based on Sec. III A, which reveals the locally and non-locally reactive behavior of a

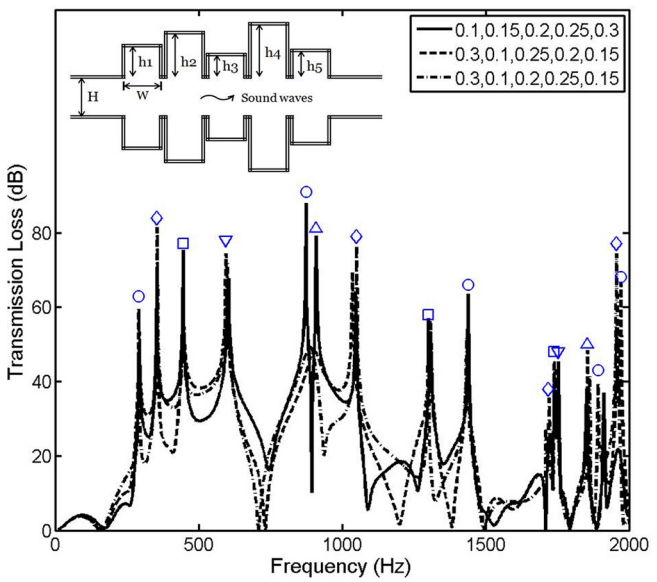

FIG. 6. (Color online) Effect of combining multiple resonator cells with varying depths. Resonant frequencies of each cell corresponding to ○—0.3 m, ◇—0.25 m, □—0.2 m, ▽—0.15 m, △—0.1 m.

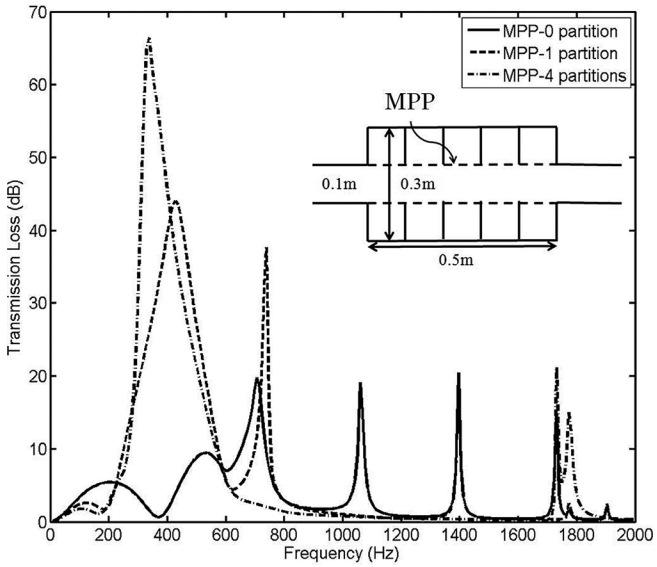

FIG. 7. TL of MPP silencers with single, dual, and five sub-chambers.

MPP under different circumstances. The hybrid attenuation mechanism of such silencer is then analyzed by separating the reactive and absorptive effect, and the influence of MPP parameters is discussed.

1. Locally reactive and non-locally reactive behavior of MPPs

When MPPs are added to the reactive silencers in Fig. 4, the side-branch cavity and the main chamber is separated by an impedance surface corresponding to the MPP. The MPP parameters used in the simulation are $t = d = 1$ mm with perforation ratio $\sigma = 1\%$. Using the proposed formulation in Sec. II, the predicted TLs corresponding to three MPP silencers with single, dual, and five chambers are presented in Fig. 7.

For the first case with no partition, comparison with the TL of the empty chamber without MPP in Fig. 4 shows that MPP has almost no effect in the low frequency range below 400 Hz, and only generates narrow TL peaks after this frequency. The MPP seems to exert marginal influence on the empty chamber. To explain this, the sound pressure field inside the silencer at $f = 380$ Hz is plotted in Fig. 8, where the pressure distribution inside the duct and side-branch is seen to be almost in phase. Since the vibration of air mass inside perforated holes depends on the pressure difference across the MPP surface, the added MPP can hardly provide any sound dissipation in such circumstance. This so-called "non-locally reactive" behavior of a MPP should be particularly noted. This indicates that by simply adopting a MPP with backing cavity system as a sound absorption device may not be effective for duct silencing purpose in real industrial applications, due to the non-locally reactive behavior of MPP. Meanwhile, only considering the absorption ratio of conventional MPP absorber configuration[17] (with a backing cavity under normal incidence) may lead to wrong estimations on its actual performance.

When solid partitions are added inside the backing cavity, the combined effect of a MPP with internal partitions is shown

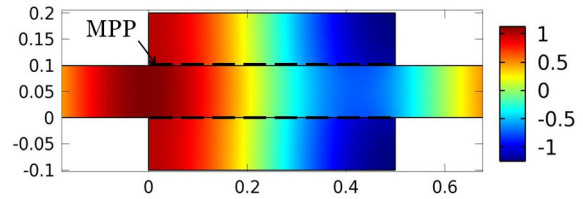

FIG. 8. (Color online) Sound pressure distribution inside the silencer with MPP and without partition, the first TL trough at $f = 380$ Hz.

in Fig. 7. With one pair of partitions, the sound pressure field inside the side-branch cavity is segmented from the middle. The induced pressure difference on both sides of a MPP causes the effective vibration of the hole mass, resulting in a TL peak near 400 Hz due to effective energy dissipation. With more pairs of partitions, the side-branch can be viewed as an array of unit cells, and the resulted TL is again an accumulative effect of all the cells connected in series. It is also found that the TL curve is roughly in accordance with the absorption coefficient of a unit cell, which takes the basic structure of a MPP absorber with a backing-cavity.[17] According to Wu,[25] if the distance between the backing partitions is smaller than half of the acoustic wavelength, the sound propagation in the y and z axes (Fig. 3) can be neglected. Therefore, the unit cell with a MPP can be approximated as a "locally reacting" boundary surface, whose normal impedance is an *a priori* quantity. In practice, this may be achieved by partitioning the backing-cavity behind a MPP using honeycomb structures.[23]

2. Parametric influences and hybrid attenuation mechanism

To achieve better silencer design, the influence of MPP parameters on the silencing performance is studied. According to Maa,[17] the surface impedance of a MPP depends on the hole diameter d, panel thickness t, and perforation ratio σ. Equation (4) shows that the hole resistance is

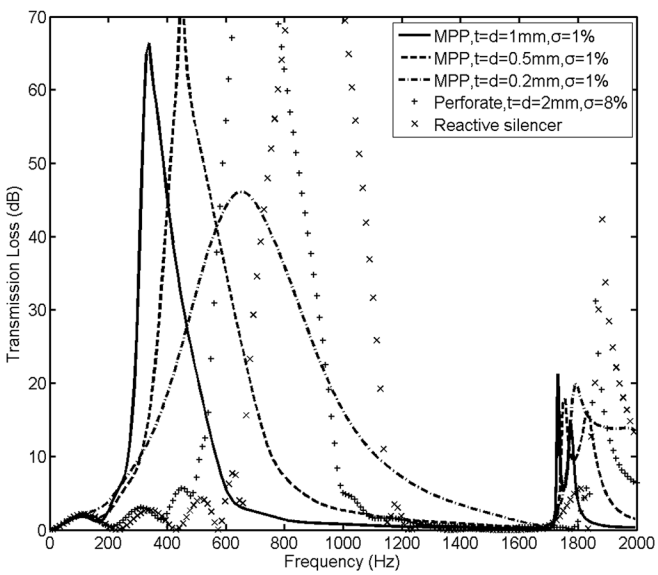

FIG. 9. Influence of varying MPP hole diameters and transitional behavior with increasing hole diameters.

proportional to the first order of panel thickness and second order of hole diameter, which means that controlling MPP impedance by adjusting the hole diameter is more effective than thickness. On the other hand, as reported from the MPP manufacturer, the hole diameter and panel thickness are usually made equal due to manufacturing constraints. Therefore, the present study combines d and t as a single variable, i.e., $d = t$.

In Fig. 9, the influence of the hole diameter is shown by comparing three MPP cases with 1, 0.5, and 0.2 mm hole diameters, respectively, where the perforation ratio is kept the same at 1%. The side-branch cavity (0.5 m in length) is divided into five sub-chambers using solid partitions. It can be seen from the comparison that with decreasing hole diameter, the narrow TL peak becomes flattened and widened, leading to a better broadband attenuation performance. The reason is that a smaller hole diameter induces higher acoustic resistance, which is most effective in widening the absorption bandwidth.

The transition phenomenon from a dissipative MPP silencer to a reactive silencer with increasing hole size can also be seen in Fig. 9. Note that when the hole diameter becomes greater than 1 mm, the Maa's formula in calculating its characteristic impedance is less accurate. Therefore, in the simulations, the MPP hole impedance [Eq. (4)] is replaced by the perforated hole impedance:[11,13]

$$Z_p = 0.006\rho_0 c_0 + j\rho_0\omega(t + 0.75d). \tag{25}$$

It can be seen that when d is increased to 2 mm, the TL peak is moved to a higher frequency. Continuously increasing the hole diameter, the surface impedance of the perforated panel is comparable to air, and the TL curve is almost equivalent to the reactive silencer in Fig. 4. This implies that the perforated duct liner with relatively large holes can be used to guide the flow and reduce back pressure in reactive silencers, such as the one presented in Fig. 6, while exerting negligible influence on the desired TL performance.

The hybrid noise attenuation mechanism is captured by separating the reflected and absorbed sound energy. The reflection and absorption coefficients (R and α, respectively) corresponding to the three MPP cases are presented in Fig. 10. A comparison between TL curve (Fig. 9) and the corresponding R and α curve (Fig. 10) allows identifying the dominant effect of the MPP silencer. For the sake of analysis, we define a stop band providing a minimum TL of 10 dB. With a small MPP hole size ($d = 0.2$ mm), Fig. 9 shows a stop band roughly from 450–1200 Hz. It can be seen from Figs. 10(a) and 10(b) that, within roughly the same frequency band, the reflection remains rather low ($R < 0.2$), while the absorption is strong ($\alpha > 0.8$). It is obvious that the dissipative effect dominates in this case. On the contrary, with a large hole size ($d = 1$ mm), a narrow stop band is produced, roughly ranging from 300–600 Hz. Within the same frequency band, a strong reflection occurs [Fig. 10(a)] along with a much weakened absorption [Fig. 10(b)]. In this case, the silencing performance of the silencer is mainly due to the reactive effect. The case with intermedia hole size ($d = 0.5$ mm) is a combination of reactive effect and

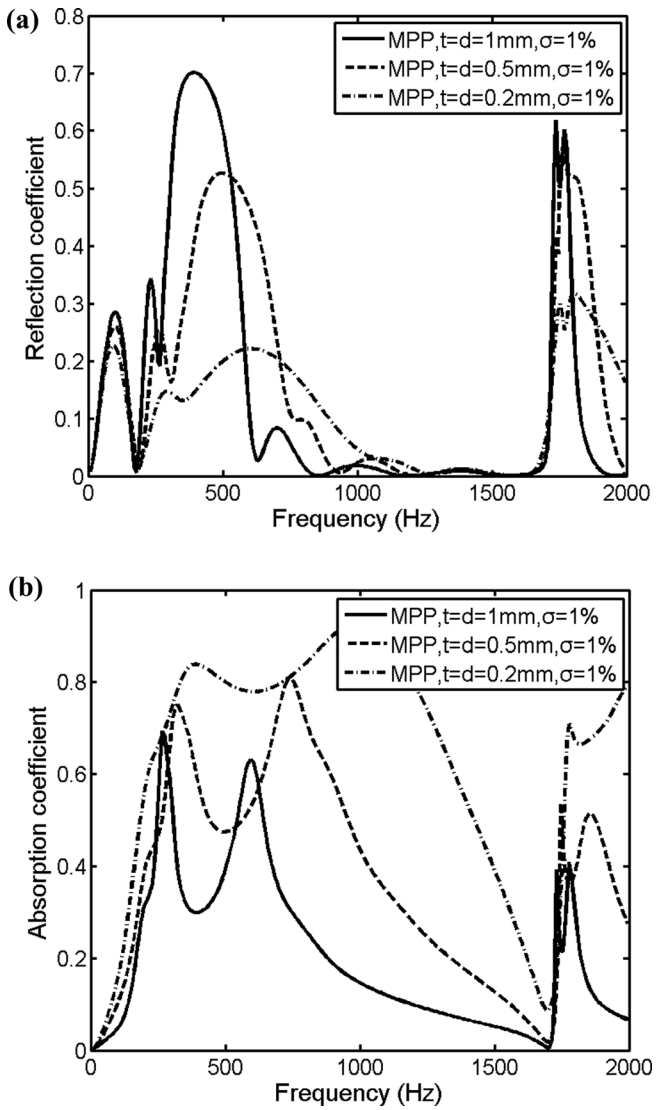

FIG. 10. Hybrid mechanism of MPP silencer: (a) Reflection coefficient representing the reactive effect; (b) absorption coefficient representing the dissipative effect.

dissipative effect. It is worth noting that the above analyses neglect the effect of mean flow inside the silencer. In the presence of air flow, Rao and Munjal[34] showed that normal perforated holes (> 1 mm) can be also dissipative due to an increased acoustic resistance.

As to the influence of perforation ratio, Fig. 11 presents three MPP cases with varying perforation ratios from 0.2% to 1%. It can be seen that the TL is very sensitive to the perforation ratio, since the MPP surface impedance is always inversely proportional to σ. The above analysis suggests that an optimal tuning of MPP parameters should always consider the hole diameter and perforation ratio together.

3. Optimization study

Owing to the flexibility and calculation efficiency offered by the proposed formulation, an optimization example based on the two MPP variables d and σ is carried out in this section. According to Eq. (19), the silencer TL is

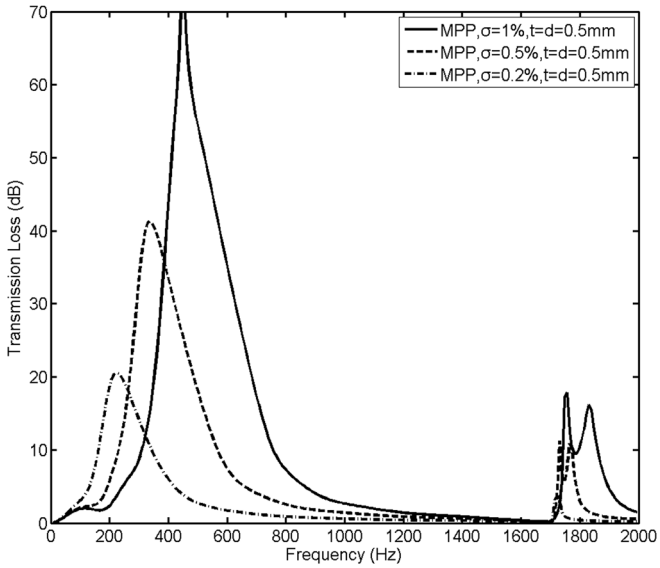

FIG. 11. Influence of varying MPP perforation ratios.

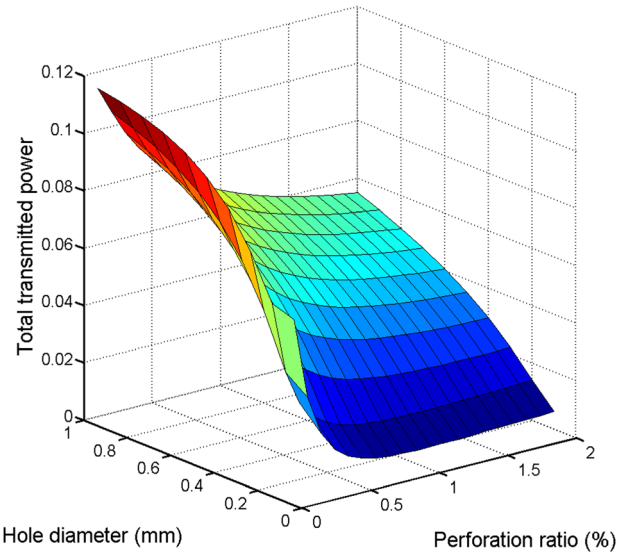

FIG. 12. (Color online) An optimization example targeting the frequency range from 200 to 1400 Hz.

calculated by the relative ratio between the incident sound power at the inlet and the transmitted power at the outlet. Since the incident power is a fixed value [Eq. (20)], the overall silencing performance within a particular frequency range can be assessed by summing up the transmitted power at all frequencies, calculated via Eq. (21).

The first case attempts to optimize the TL from 200 to 1400 Hz, which covers nearly three octave bands. The constraint on the hole diameter is set as 0.1 to 1 mm, with an increment of 0.1 mm (10 points in total), and that of the perforation ratio varies from 0.1% to 2%, with an increment of 0.1% (20 points). The full optimization process using the proposed approach is presented in Fig. 12. For each combination of d and σ, the transmitted power at 121 frequency points (with a linear frequency step of 10 Hz) are summed up as the "total transmitted power." The lower value means better overall silencing performance. Owing to the modular nature of the proposed formulation, only MPP mobility in Eq. (10) is re-calculated during the optimization loop, while subsystem PTFs of all the other acoustic domains are unchanged. As such, the computational time for nearly 2.5×10^4 calculations in total is typically less than 10 min using a personal computer.

From the optimization map, the minimal point is identified at $t = d = 0.1$ mm, $\sigma = 1.1\%$, and the resulted TL is plotted in Fig. 13. It can be seen that such MPP parameters provide a broadband TL characteristics compared with the reactive silencer without MPP (Fig. 4), with stop band covers from 280 to 1360 Hz. Following the same procedure, another optimization case targets a narrower frequency band from 300 to 900 Hz. The optimization gives optimal combination of $t = d = 0.2$ mm, $\sigma = 0.8\%$. In Fig. 13, the optimized silencer shows better performance than the previous one in the target frequency range.

The tuning of MPP parameters demonstrates the capability of the proposed approach in performing system optimization. It is noted that for practical silencer design, the backing-cavity dimension of unit cells can also be included as optimization parameters, as verified in Sec. III A.

4. Partial MPP with opening

To further demonstrate the capability of the proposed formulation, a complex silencer configuration comprising partial MPPs is studied, where the MPP facing of a unit cell is partially opened with an aperture. The co-existence of a MPP and an aperture among a mixed separation interface is treated using a recently proposed Compound Interface technique,[33] with the aperture being formulated as an equivalent virtual panel element.[35] In the simulation, 1/10 or 2/10 of the MPP surface area is allowed to open, as sketched in Fig. 14. The MPP parameters which exhibit the best broadband performance in Sec. III B 3 are used, i.e., $t = d = 0.1$ mm, $\sigma = 1.1\%$.

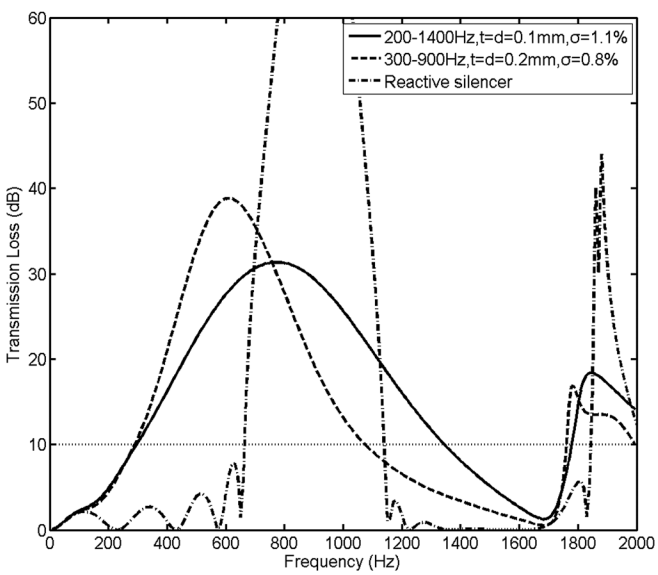

FIG. 13. Optimized silencer TLs for two different frequency ranges.

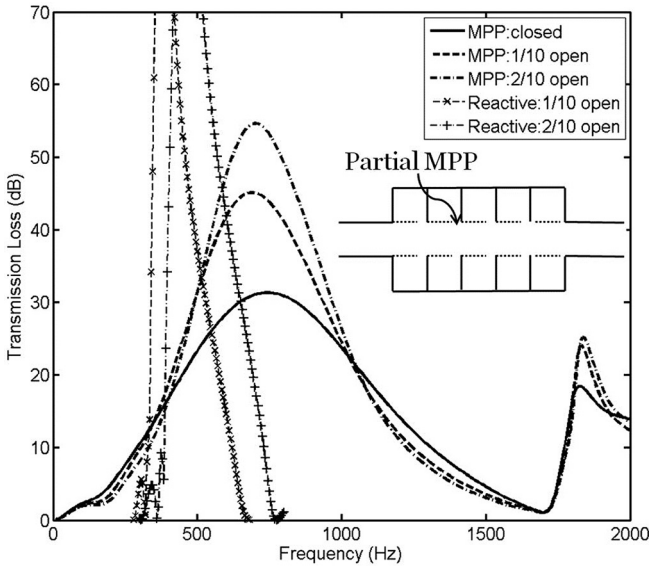

FIG. 14. Effect of partial MPPs with openings on the silencing performance.

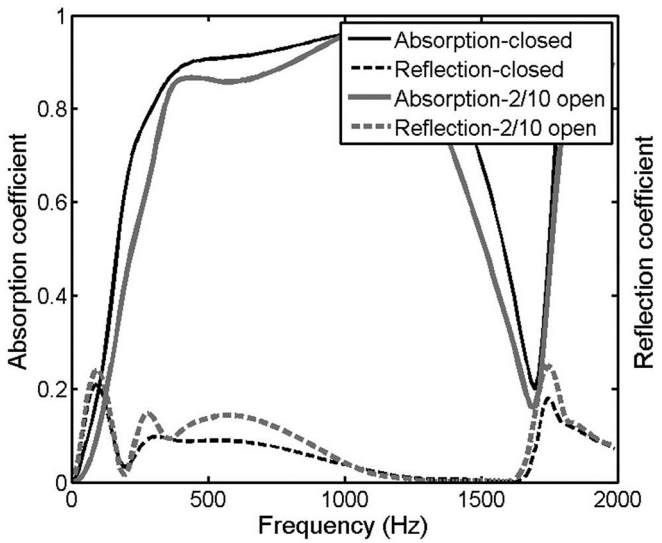

FIG. 15. With partial MPP, the reactive effect is enhanced, while the dissipative effect is weakened.

The corresponding TL curves are presented in Fig. 14. Comparing to the silencer with closed MPP, the TL performance near the peak region is lifted up, without sacrificing too much at other frequencies. This means that a partial MPP can further enhance the desired silencing performance near the target frequencies. If the partial MPPs are replaced by partial solid panels, the TL characteristics of the reactive silencers[32] are also compared in Fig. 14. As expected, the reactive silencers can only provide narrow TL stop bands. This shows that by introducing micro-perforations to the reactive silencer, the narrow TL can be greatly improved to a broadband behavior.

To understand the underlying mechanism, the sound reflection and absorption coefficients corresponding to the partial and closed MPP configurations are compared in Fig. 15. It can be seen that with partial MPP, the absorption effect is not as effective as the closed one, while the reflection effect is stronger. The enhanced reactive behavior can be explained by the direct connections between the duct and backing cavities in the presence of openings, where the resonator effect due to internal partitions becomes more dominant. On the other hand, the weakened dissipative effect with openings is possibly due to induced pressure balance across the MPP surface,[33] which lowers the extent of air mass vibration inside holes. Another plausible reason might be a reduction in the effective absorbing surface area due to partial MPPs.

IV. EXPERIMENTAL VALIDATION

To further confirm the calculation using the proposed formulation, a MPP silencer as shown in Fig. 16(a) is constructed and tested. The experimental setup is based on the four-microphone, two-load method, as detailed in Ref. 32. The dimension of the expansion chamber is the same as the one used in Sec. III, and the aluminum MPP panels 0.35 mm thick are punched with 0.25 mm holes, with a perforation ratio of 1.2%.

In Fig. 16(b), the calculated TL using the proposed approach is presented and compared with the measured results, which shows good agreement. The discrepancies mainly come from the possible experimental error, and imperfection of the MPP. It can be seen that such MPP silencer with small expansion ratio provides an acoustic stop

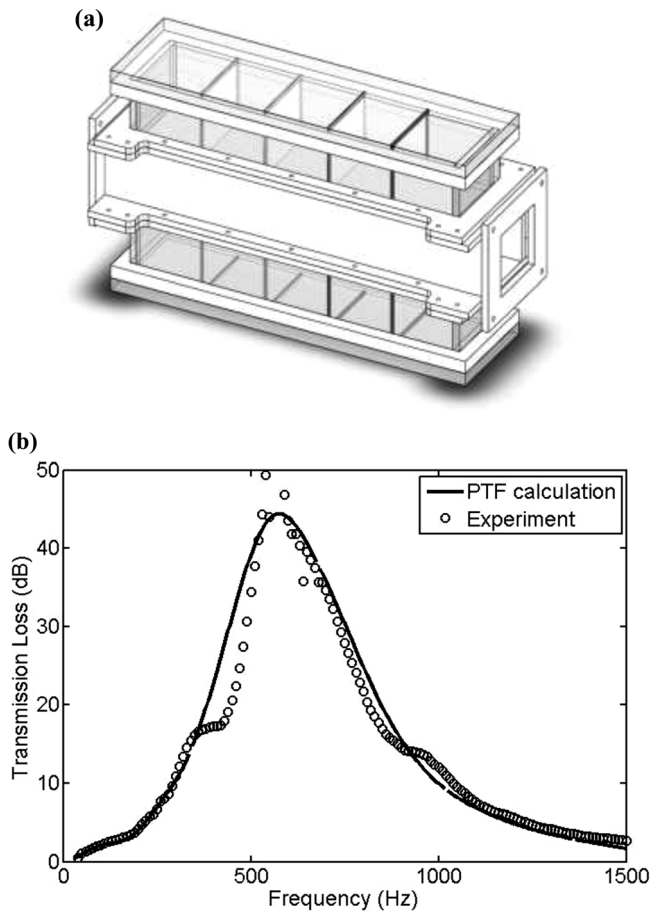

FIG. 16. (a) Drawing of the MPP silencer; (b) comparison between the predicted TL using the PTF approach and experimental result.

band from 300 to 1050 Hz, with TL greater than 10 dB, which exhibits great potential in the design of practical noise control systems.

V. CONCLUSIONS

A 3D sub-structuring approach, along with a unit cell treatment, is proposed to model expansion chamber silencers with internal partitions and MPPs. The side-branch configuration is treated as a combination of unit cells connected in series, each comprising a MPP facing and a backing cavity. The proposed formulation is employed to study various MPP silencer configurations, which demonstrates its capability and flexibility in handling such systems. The accuracy and convergence of the calculations are validated against FEM analyses and experiments.

The hybrid noise attenuation mechanism of the MPP silencer is revealed. In principle, a typical MPP silencer exhibits both dissipative and reactive effects to the incoming sound. As a whole, a MPP under grazing incidence dissipates sound energy into heat by means of air mass vibration inside holes, while the backing partitions provide a reactive effect by reflecting sound waves to the upper-stream. Depending on the size of the perforation hole, the noise attenuation can be dominated by one or the other. Typically, with a small hole size, dissipation dominates, usually resulting in a wider TL stop band. In the other extreme case with a large hole size, reactive effect dominates, leading to a much narrower and pronounced TL stop band in a lower frequency range. For a broadband sound absorption, the hole diameter, together with the perforation ratio and other parameters, can be optimized to balance the dissipative and reactive effect, for ultimately achieving the desired noise attenuation performance within a prescribed frequency region. It is demonstrated that the proposed formulation, together with the unit cell treatment, due to the modular nature, allows not only a quick estimation of acoustic stop bands provided by each cell and the assembled system, but also a flexible tuning of existing design and optimization in a flexible, accurate, and cost effective manner.

As a final remark, it should be mentioned that the numerical studies reported in this paper neglect the possible presence of the internal flow, whose influence on both the MPP behavior and the silencing performance of the silencer may not be negligible when the flow speed is high. This shows the necessity for revisiting the conventional impedance formula of the MPP, understanding its energy dissipation mechanism, as well as re-evaluating the noise attenuation performance of the MPP-based silencer design in the presence of high-speed flow.

ACKNOWLEDGMENT

The authors wish to acknowledge a grant from the Research Grants Council of Hong Kong Special Administrative Region, China (Grant No. PolyU 5103/13E).

[1]A. Selamet and Z. L. Ji, "Acoustic attenuation performance of circular expansion chambers with extended inlet/outlet," J. Sound Vib. **223**, 197–212 (1999).
[2]A. Selamet, F. D. Denia, and A. J. Besa, "Acoustic behavior of circular dual-chamber mufflers," J. Sound Vib. **265**, 967–985 (2002).
[3]Z. L. Ji, "Acoustic attenuation performance analysis of multi-chamber reactive silencers," J. Sound Vib. **283**, 459–466 (2005).
[4]J. W. Lee and Y. Y. Kim, "Topology optimization of muffler internal partitions for improving acoustic attenuation performance," Int. J. Numer. Mech. **80**, 455–477 (2009).
[5]J. W. Lee and G. W. Jang, "Topology design of reactive mufflers for enhancing their acoustic attenuation performance and flow characteristics simultaneously," Int. J. Numer. Mech. **91**, 552–570 (2012).
[6]C. Q. Howard, B. S. Cazzolato, and C. H. Hansen, "Exhaust stack silencer design using finite element analysis," Noise Control Eng. **48**, 113–120 (2000).
[7]X. Wang and C. M. Mak, "Wave propagation in a duct with a periodic Helmholtz resonators array," J. Acoust. Soc. Am. **131**, 1172–1182 (2012).
[8]S. H. Seo and Y. H. Kim, "Silencer design by using array resonators for low-frequency band noise reduction," J. Acoust. Soc. Am. **118**, 2332–2338 (2005).
[9]L. Huang, "Broadband sound reflection by plates covering side-branch cavities in a duct," J. Acoust. Soc. Am. **119**, 2628–2638 (2006).
[10]R. J. Astley and A. Cumming, "A finite element scheme for attenuation in ducts lined with porous material: Comparison with experiment," J. Sound Vib. **116**, 239–263 (1987).
[11]I. Lee, A. Selamet, and N. T. Huff, "Acoustic impedance of perforations in contact with fibrous material," J. Acoust. Soc. Am. **119**, 2785–2797 (2006).
[12]I. Lee, A. Selamet, and N. T. Huff, "Impact of perforation impedance on the transmission loss of reactive and dissipative silencers," J. Acoust. Soc. Am. **120**, 3706–3713 (2006).
[13]Z. L. Ji, "Boundary element analysis of a straight-through hybrid silencer," J. Sound Vib. **292**, 415–423 (2006).
[14]T. W. Wu, C. Y. R. Cheng, and Z. Tao, "Boundary element analysis of packed silencers with protective cloth and embedded thin surfaces," J. Sound Vib. **261**, 1–15 (2003).
[15]G. Lou, T. W. Wu, and C. Y. R. Cheng, "Boundary element analysis of packed silencers with a substructuring technique," Eng. Anal. Bound. Element. **27**, 643–653 (2003).
[16]T. W. Wu, C. Y. R. Cheng, and P. Zhang, "A direct mixed-body boundary element method for packed silencers," J. Acoust. Soc. Am. **111**, 2566–2572 (2002).
[17]D. Y. Maa, "Potential of micro-perforated panel absorber," J. Acoust. Soc. Am. **104**, 2861–2866 (1998).
[18]C. Wang, L. Cheng, J. Pan, and G. H. Yu, "Sound absorption of a micro-perforated panel backed by an irregular-shaped cavity," J. Acoust. Soc. Am. **127**, 238–246 (2010).
[19]C. Yang, L. Cheng, and J. Pan, "Absorption of oblique incidence sound by a finite micro-perforated panel absorber," J. Acoust. Soc. Am. **133**, 201–209 (2013).
[20]L. Maxit, C. Yang, L. Cheng, and J. L. Guyader, "Modeling of micro-perforated panels in a complex vibro-acoustic environment using patch transfer function approach," J. Acoust. Soc. Am. **131**, 2118–2130 (2012).
[21]F. Asdrubali and G. Pispola, "Properties of transparent sound-absorbing panels for use in noise barriers," J. Acoust. Soc. Am. **121**, 214–221 (2007).
[22]S. H. Park, "Acoustic properties of micro-perforated panel absorbers backed by Helmholtz resonators for the improvement of low-frequency sound absorption," J. Sound Vib. **332**, 4895–4911 (2013).
[23]J. Liu and D. W. Herrin, "Enhancing micro-perforated panel attenuation by partitioning the adjoining cavity," Appl. Acoust. **71**, 120–127 (2010).
[24]D. Herrin, J. H. Liu, and A. Seybert, "Properties and applications of micro-perforated panels," J. Sound Vib. **45**, 6–9 (2011).
[25]M. Q. Wu, "Micro-perforated panels for duct silencing," Noise Control Eng. **45**, 69–77 (1997).
[26]X. N. Wang, Y. S. Choy, and L. Cheng, "Hybrid noise control in a duct using a light micro-perforated plate," J. Acoust. Soc. Am. **132**, 3778–3787 (2012).
[27]S. Allam and M. Åbom, "A new type of muffler based on microperforated tubes," J. Vib. Acoust. **133**, 031005 (2011).
[28]M. Åbom and S. Allam, "Dissipative silencers based on micro-perforated plates," SAE [Tech. Pap.] **6**, Paper 2013-24-0071 (2013).
[29]M. Ouisse, L. Maxit, C. Cacciolati, and J. L. Guyader, "Patch transfer functions as a tool to couple linear acoustic problems," J. Vib Acoust. **127**, 458–466 (2005).

[30]J. D. Chazot and J. L. Guyader, "Prediction of transmission loss of double panels with a patch-mobility method," J. Acoust. Soc. Am. **121**, 267–278 (2007).
[31]X. Yu, L. Cheng, and J. L. Guyader, "Vibroacoustic modeling of cascade panels system involving apertures and micro-perforated elements," in *20th International Congress on Sound & Vibration* (2013).
[32]X. Yu and L. Cheng, "Duct noise attenuation using reactive expansion chamber silencer with various internal configurations," J. Sound Vib. **335**, 229–244 (2015).
[33]X. Yu, L. Cheng, and J. L. Guyader, "Modeling vibroacoustic systems involving cascade open cavities and micro-perforated panels," J. Acoust. Soc. Am. **136**, 659–670 (2014).
[34]K. N. Rao and M. L. Munjal, "Experimental evaluation of impedance of perforates with grazing flow," J. Sound Vib. **108**, 283–295 (1986).
[35]X. Yu, L. Cheng, and J. L. Guyader, "On the modeling of sound transmission through a mixed separation of flexible structure with an aperture," J. Acoust. Soc. Am. **135**, 2785–2796 (2014).